Melting of Colloidal Crystal Films

Y. Peng,[1] Z. Wang,[1] A. M. Alsayed,[2,3] A. G. Yodh,[2] and Y. Han[1,*]

[1]Department of Physics, Hong Kong University of Science and Technology, Clear Water Bay, Hong Kong, China
[2]Department of Physics and Astronomy, University of Pennsylvania, 209 South 33rd Street, Philadelphia, Pennsylvania 19104, USA
[3]Complex Assemblies of Soft Matter, CNRS/UPENN/Rhodia UMI 3254, Bristol, Pennslyvania 19007, USA

(Received 29 January 2010; revised manuscript received 26 March 2010; published 18 May 2010; corrected 20 May 2010)

We study melting mechanisms in single and polycrystalline colloidal films composed of diameter-tunable microgel spheres with short-ranged repulsive interactions and confined between two glass walls. Thick films (>4 layers), thin-films (4 layers), and monolayers exhibit different melting behaviors. Thick films melt from grain boundaries in polycrystalline solid films and from film-wall interfaces in single-crystal films; a liquid-solid coexistence regime is observed in thick films but vanishes at a critical thickness of 4 layers. Thin solid films (2 to 4 layers) melt into the liquid phase in one step from both grain boundaries and from within crystalline domains. Monolayers melt in two steps with a middle hexatic phase.

DOI: 10.1103/PhysRevLett.104.205703 PACS numbers: 64.70.D , 64.60.Cn, 82.70.Dd

The effects of confinement and dimensionality on the properties of thin crystalline films are vitally important for lubrication and adhesion technology [1]. On a more fundamental level, confinement and dimensionality profoundly affect crystal melting [2,3]. In two-dimensions (2D), for example, melting sometimes proceeds in two steps, from crystal to the so-called hexatic phase and then from hexatic to liquid phase [4,5]. Such behavior is qualitatively different from well-known one-step first-order bulk melting in three dimensions (3D). Thin crystalline films are not two-dimensional but are not fully bulk-like either. As such, the melting behavior of thin solid films presents interesting new questions and challenges for both theory and experiment. To date, a few experiments in atomic and molecular thin films have begun to explore these issues. Thin-film melting, for example, was observed to occur via surface melting at solid-vapor interfaces and progress through the film to the substrate [6,7]. Fully confined atomic films without solid-vapor interfaces have not been studied, however, and therefore simple questions about how grain-boundary melting might compete with interfacial melting between film and substrate [2] have never been addressed. Moreover, atomic thin-film melting experiments rarely provide microscopic details with single-atom resolution.

Here, we explore melting mechanisms in thin single- and polycrystalline colloidal films. Colloids are useful thermodynamic model systems for melting studies in films; the trajectories of all particles in the field of view are measurable by video microscopy with single-particle resolution, and the interparticle interactions are simple and well understood. Thus far, phase diagrams for hard spheres between two walls in the relatively thin-film limit (<6 layers) have been determined by simulation [8,9], and experiments have identified predicted static crystalline structures [10–12]. Their melting transitions, however, have not been measured because it is difficult to drive the melting transition *in situ* using conventional colloids. The present melting experiments are facilitated by novel *N*-isopropylacrylamide (NIPA) colloidal microgel spheres whose diameter can be tuned by temperature [13] to drive volume-fraction dependent melting transitions [14–16]. Interestingly, we find that thick films (>4 layers), thin films (4 layers), and monolayers exhibit different melting behaviors.

Rhodamine-labeled fluorescent NIPA spheres were synthesized with <3% polydispersity and suspended in 1 mM acetic acid buffer solution. The short-ranged steric repulsive pair potential, $u(r)$, was derived from a liquid-structure analysis of dilute monolayers [17] (see Fig. S1 of Ref. [18]). The effective diameter, , at $u( ) = 1k_BT$, varied linearly from 1.27 m at 24.1 C to 1.14 m at 28.0 C. Many colloidal layers can be observed, even with bright-field microscopy [15]. Very thick samples with more than 20 layers were loaded into 18 3 H mm^3 glass channel samples, where H is the channel thickness. In this case, the colloidal suspensions flow align during loading, and single crystals can be obtained by further annealing (e.g., temperature cycling). Films with fewer than 20 layers were made by direct deposition of colloidal suspension between two glass walls. These samples were sealed, and a fixed sample cell thickness was thereby frozen-in. For example, 1.5 L colloid usually formed two layers at the sample center and four layers at the sample edges over an 18 18 mm^2 area; thus, the walls are essentially parallel over the full 0.1 mm microscope field of view. All glass surfaces were rigorously cleaned so that particles did not stick to the walls.

The particles in samples of 20 layers, or less, self-assembled into polycrystalline solids with a typical domain size of 10–100 m. Such small domain sizes introduce finite-size effects which can become important in thin-film melting [19]. To avoid these finite-size effects, we applied a vertical vibration to the sample; this vibration induced

periodic flow in the sample and effectively annealing the sample into very large domains with 10^6 particles per layer for which finite-size effects are expected to be negligible [19]. In thin films (4-layer), typical measurements were performed on (60 m)^2 central areas (2300 particles) within a 1 mm^2 sized domain. Finally, before every experiment, we cycled the temperature slightly below the melting point in order to anneal small defects away and release possible pressure build up.

The temperature controller on the microscope has 0.1 C resolution, and we increased the sample temperature in 0.2 C/steps. At each temperature, 5 minutes of video were recorded in bright-field microscopy, 2 to 4 minutes of video were recorded for each layer in confocal microscopy, and 1 to 10 full 3D confocal scans of the static structure were taken. Video rates were 30 frames/sec in bright-field microscopy and, typically, 7.5 frames/sec in confocal microscopy. The particle positions in each frame were obtained using standard 2D and 3D image analysis algorithms [20].

First, we describe the differences in melting between single and polycrystalline thick films. Three-dimensional polycrystalline crystals have been demonstrated to melt from grain boundaries [15], but similar melting experiments on 3D single colloidal crystals have not been carried out [21]. For the very thick, >20-layer films, we successfully annealed whole 18 3 H mm^3 samples into single face-centered cubic (fcc) crystals without grain boundaries. These very-thick-film single crystals exhibited interfacial melting; i.e., melting started from film surface (111) planes adjacent to the glass walls and then propagated into the bulk. In contrast, thick polycrystalline samples melted from grain boundaries; interfacial melting at the flat glass walls is suppressed [15]. This observation indicates that the interfacial energy between the (111) plane and the flat glass wall in single crystals is lower than the interfacial energies of grain boundaries in polycrystalline samples. Melting never started from within the bulk of the single-crystal thick films because spheres near the flat glass walls have larger local free volumes than spheres in the bulk material and therefore have greater propensity to melt.

Moving to fewer layer polycrystalline films, we have found that thick films (>4 layers) and thin films (4 layers) exhibit qualitatively different behaviors. Thick films start melting at grain boundaries, and then the fluid propagates into adjacent crystal domains, see Fig. 1(a). If the film is not too thick (e.g., $4 < H < 10$ layers), and the domain size is large and the heating rate fast, then the melting starts from both grain boundaries and from within the thick film crystalline domains, see the liquid "strip" and "lake" in Figs. 1(b) and 1(c). Fluids in the lakelike domains nucleate at the walls and then grow into the bulk, forming cylinderlike liquid domains embedded within a larger crystalline domain. The "lakes" will slowly diffuse toward nearby liquid "strips" wherein they irreversibly merge. Finally, we have found that large crystalline islands coexist with liquid in equilibrium.

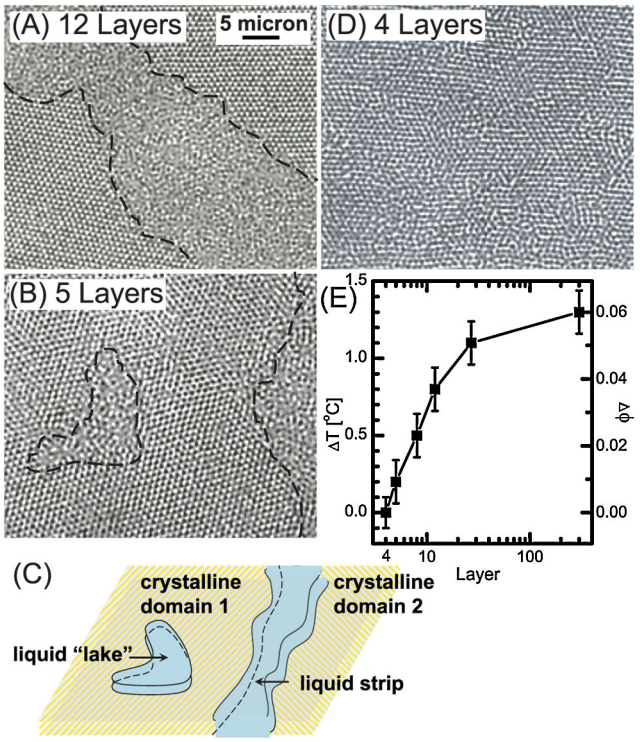

FIG. 1 (color online). (a) A 12-layer thick polycrystalline solid melts from grain boundaries. (b) A 5-layer thick polycrystalline solid melts from both grain boundaries and from within the crystalline domains. Left loop: a liquid "lake." Right hand side dashed line: a liquid "strip" between two domains. (The liquid domain on the right extends out of the image.) (c) Three-dimensional schematic of (b). (d) A 4-layer polycrystalline solid melts from random positions within the sample. Small defects do not nucleate into large liquid clusters and domains. (e) The liquid-solid coexistence regime (expressed as the temperature window interval T or packing fraction interval for coexistence) decreases with the film thickness.

A competition between surface layer and grain-boundary energies determines where polycrystalline film melting begins. As the samples thin, the grain-boundary regions become narrower bands and are less favorable for liquid nucleation. We found grain-boundary melting to be more favorable in >4-layer polycrystals, and interfacial and grain-boundary melting to be equally favorable in 4-layer thin-film polycrystalline solids. In other words, thick films melt by generating liquid "strips" at grain boundaries which gradually expand as the volume fraction decreases, while thin-film crystals abruptly melt at a critical volume fraction by generating many small defects and transient chainlike clusters at both grain boundaries and within crystalline domains, see Fig. 1(d) and Figs. S2, S3 in [18]. Such differences were robust across tens of samples made from different batches of microgel particles. Evidently, the thinner films are more vulnerable to long wavelength density fluctuations [4], and, below 4 layers, thermal fluctuations become strong enough to break up large crystalline domains into small crystalline patches and thus prevent small defects from condensing into large

liquid domains (e.g., such as "strips" or "lake"). These behaviors have also been observed in 2D melting experiments [16,22].

We next explore how liquid-solid coexistence changes with the film thickness. For 3D samples of hard spheres [23], the solid-liquid coexistence regime is well known to range from 54.5% to 49.5% in volume fraction. In our thickest films, the coexistence regime was measured to range from 53.9% to 47.9%, when defining volume fractions using the particle diameters at $u(r) = 1k_BT$. As film thickness becomes smaller, however, we find that the liquid-solid coexistence regime decreases with film thickness and vanishes at a critical thickness of 4 layers, see Fig. 1(e). Evidently, the liquid packing fraction in the thinner films is relatively closer to the solid packing fraction because the liquid is stratified into well separated layers and the films are more ordered near the walls. Consequently, the coexistence regime decreases with the film thickness and melting becomes 2D-like below 4 layers. In 4-layer films, melting within domains produces small crystalline patches mixed with small liquid/defect clusters in equilibrium, a behavior which is qualitatively different from that of solid-liquid phase separation in the 3D coexistence regime. We assign this mixture phase to be a liquid based on the analyses in Fig. 2 and below. The lack of liquid-solid coexistence in the very thin films stands in contrast to observations from simulation about hard-sphere monolayer and thin-film melting [8,9], perhaps because microgel particles are soft. Melting of monolayers and thin films is known to be sensitive to particle interactions [3,8,24].

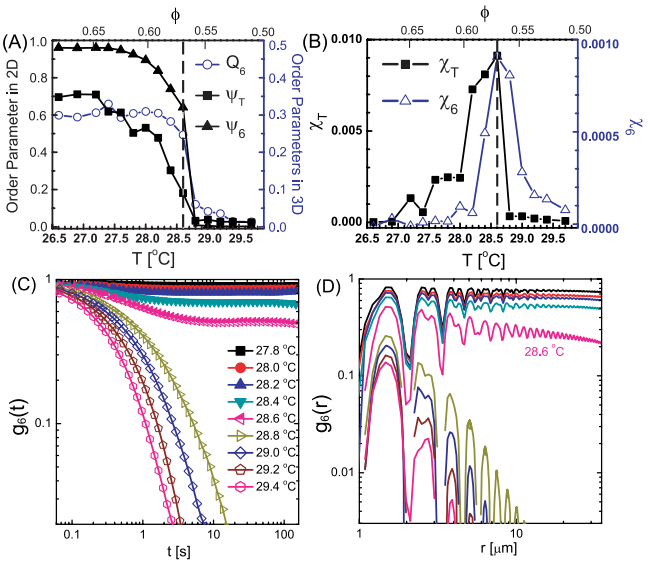

FIG. 2 (color online). 2△ crystal melting. Here, the results are derived from one of the two surface layers. (a) Two-dimensional translational, 2D and 3D orientational order parameters: ψ_T, ψ_6, and Q_6, respectively, as a function of sample temperature T and packing fraction . (b) Translational and orientational susceptibilities $_T$ and $_6$. (c) Orientational correlation functions $g_6(t)$ in time. (d) Orientational correlation functions $g_6(r)$ in space.

Finally, since the 2- to 4-layer films and monolayers appear to have the same qualitative melting behavior, it is natural to inquire about whether such thin films also exhibit an intermediate hexatic phase, as in 2D melting [16]. Because the thin films melt uniformly, we can quantitatively measure their structure and dynamics. Thin-film colloidal crystals confined between two walls exhibit a cascade of phases: 1 △− 2□ 2 △− 3□ 3 △− 4□ as a function of increasing wall separation [10]. Here, 1△ denotes monolayer triangular lattice, 2□ denotes two-layer square lattice, etc. We studied melting of 2 △ , 3□, 3 △ , and 4 □ thin-film crystals. The vertical density profiles clearly show that particles stratify into layers even in the liquid phase. Thus, we could identify the sample phase layer by layer at each temperature. In practice, layer-by-layer 2D imaging has better spatial and temporal resolution and better statistics than 3D imaging. We also analyzed 3D order parameters [25] from which we obtained the same melting point as determined from the 2D analyses.

To carry out this procedure, we labeled each particle in our image analysis by $\{x_j, y_j, t, \psi_{6j}(\text{or } \psi_{4j}), \psi_{Tj}\}$ [4,16]. Here, t is time, $\psi_{6j} = (\sum_{k=1}^{nn} e^{6i\theta_{jk}})/nn$ (or $\psi_{4j} = (\sum_{k=1}^{nn} e^{4i\theta_{jk}})/nn$) is the 2D orientational order parameter for sixfold (or fourfold) symmetry, and $\psi_{Tj} = e^{i\mathbf{G}\,\mathbf{r}_j}$ is the translational order parameter for particle j at position $\mathbf{r}_j = (x_j, y_j)$. $_{jk}$ is the angle of the bond between particle j and its neighbor k. nn is the number of nearest neighbors. For triangular lattices, the nearest neighbors are identified by Delaunay triangulation. For square lattices, however, nearest neighbors have to be further constrained to a distance less than $1.2a$, the midpoint between lattice constant a and second nearest-neighbor distance $\sqrt{2}a$. a is measured from the position of the first peak of the radial distribution function $g(r)$. $\mathbf{G}$ is a primary reciprocal lattice vector measured from the peak of the 2D structure factor at each temperature in the crystal phase [16].

The global order parameter is the averaged order parameter over all N particles: ψ $= (\sum_{j=1}^{N} \psi_{\alpha j})/N$ where $= 6$, 4 or T. Figure 2(a) shows the global ψ_T and ψ_6 in 2△ crystal melting. The 3D orientational order parameter Q_6 in Fig. 2(a) is calculated from spherical harmonics, see Refs. [8,25]. All the order parameters abruptly jump at 28.7 C. The transition point can also be identified from the correlation functions g (r) and g (t) of in space and time. In the Kosterlitz-Thouless-Halperin-Nelson-Young (KTHNY) theory, both $g_6(t)$ and $g_6(r)$ approach a constant in crystal (long-ranged order), decay algebraically in hexatic phase (quasi-long-ranged order), and decay exponentially in liquid phase (short-ranged order). The $g_6(t)$ in Fig. 2(c) clearly shows a crystal phase below 28.7 C and a liquid phase above 28.7 C. The $g_6(r)$ in Fig. 2(d) exhibit behavior similar to $g_6(t)$, but the crystal at 28.6 C appears to have a power-law decay. This power-law decay appears to be more indicative of a finite-size effect than a signature of hexatic phase. In fact, $g_6(t)$ at 28.6 C in Fig. 2(c) also decays algebraically at short time,

TABLE I. Summary of the melting behaviors of polycrystalline or single-crystal thin films.

L-layer thickness	$L > 4$	$1 < L$ 4	$L = 1$
grain-boundary melting	yes/-	yes/-	yes/-
interfacial melting	no [a]/yes	yes/yes	-/-
solid-liquid coexistence	yes/yes	no [b]/no [b,c]	no [b]/no [b,c]
middle hexatic phase	no/no	no [d]/no [c]	no/yes

[a]If heating is very fast, then $4 < L <$ 10-layer films can melt from the film-wall interface.
[b]Note, the liquid phase containing many small crystalline patches was not considered to be in coexistence.
[c]Expectation from polycrystalline results.
[d]Within 0.2 C (1% area fraction) uncertainty.

but becomes constant at longer times. $g_T(r)$ and $g_T(t)$ yielded consistent results.

The divergence of the susceptibility provides another signature of a phase transition. We found this method to be superior to the other methods described above because it avoids finite size or time ambiguities [16]. The susceptibility is the fluctuation of the global order parameter. We calculated in different size sub-boxes and extrapolated to the infinite-size limit [16]. In Fig. 2(b), both $_T$ and $_6$ peak at almost the same packing fraction, indicative of a one-step transition (liquid-crystal) without a middle phase (given our temperature resolution). In contrast, $_T$ and $_6$ of the *monolayer* melting peaked at different packing fractions, respectively, and thus defined a middle (hexatic) phase [16].

3□, 3△, and 4□ crystals also exhibit one-step melting, and their order parameters, correlations, and susceptibilities are similar to those of 2△ in Fig. 2. The same analysis applied to bulk layers yielded the same melting points and conclusions as for surface layers. However, we observed that surface layers melt faster than bulk layers. We observed buckled phases or prism phases [9,26] at high volume fraction. Upon decreasing the volume fraction, the buckling disappeared and the domains became normal crystal; these normal crystals melted upon further lowering of the volume fraction.

In summary, thick films (>4 layers), thin-films (4 layers), and monolayers exhibit different melting behaviors, see Table I. The solid-liquid coexistence regime decreases with the film thickness, vanishing at a critical thickness of 4 layers. In the (4 layer) regime, thin-film melting was clearly demonstrated to be a one-step transition without a middle tetratic or hexatic phase. Studies of melting of a methane films on a graphite substrate [7] reported that thick methane films (>4 layers) melt via a first-order transition and thinner films (4 layers) appear to have continuous transitions with a vanishing latent heat. It is interesting to speculate about whether the 4-layer critical thickness observed in both colloidal and molecular crystals is universal. Our observations cast new light on these problems and provide new challenges for theory.

This work was supported by RGC-601208 (Y. H.) and by the NSF DMR-0804881, MRSEC DMR-0520020, and NASA NAG-2939 (A. G. Y.)

*yilong@ust.hk

[1] C. Alba-Simionesco *et al.*, J. Phys. Condens. Matter **18**, R15 (2006).
[2] J. G. Dash, Rev. Mod. Phys. **71**, 1737 (1999).
[3] U. Gasser, J. Phys. Condens. Matter **21**, 203101 (2009).
[4] K. J. Strandburg, Rev. Mod. Phys. **60**, 161 (1988).
[5] K. Zahn, R. Lenke, and G. Maret, Phys. Rev. Lett. **82**, 2721 (1999).
[6] D.-M. Zhu and J. G. Dash, Phys. Rev. Lett. **57**, 2959 (1986); D.-M. Zhu and J. G. Dash, *ibid.* **60**, 432 (1988).
[7] M. S. Pettersen, M. J. Lysek, and D. L. Goodstein, Phys. Rev. B **40**, 4938 (1989).
[8] M. Schmidt and H. Löwen, Phys. Rev. Lett. **76**, 4552 (1996); M. Schmidt and H. Löwen, Phys. Rev. E **55**, 7228 (1997).
[9] A. Fortini and M. Dijkstra, J. Phys. Condens. Matter **18**, L371 (2006).
[10] P. Pieranski, L. Strzelecki, and B. Pansu, Phys. Rev. Lett. **50**, 900 (1983).
[11] J. A. Weiss, D. W. Oxtoby, D. G. Grier, and C. A. Murray, J. Chem. Phys. **103**, 1180 (1995); S. Neser, C. Bechinger, P. Leiderer, and T. Palberg, Phys. Rev. Lett. **79**, 2348 (1997); R. Zangi and S. A. Rice, Phys. Rev. E **61**, 660 (2000).
[12] F. Ramiro-Manzano, E. Bonet, I. Rodriguez, and F. Meseguer, Phys. Rev. E **76**, 050401(R) (2007); A. B. Fontecha, T. Palberg, and H. J. Schöpe, *ibid.* **76**, 050402 (R) (2007).
[13] R. Pelton, Adv. Colloid Interface Sci. **85**, 1 (2000).
[14] S. B. Debord and L. A. Lyon, J. Phys. Chem. B **107**, 2927 (2003); J. Wu, B. Zhou, and Z. Hu, Phys. Rev. Lett. **90**, 048304 (2003).
[15] A. M. Alsayed *et al.*, Science **309**, 1207 (2005).
[16] Y. Han, N. Y. Ha, A. M. Alsayed, and A. G. Yodh, Phys. Rev. E **77**, 041406 (2008).
[17] S. H. Behrens and D. G. Grier, Phys. Rev. E **64**, 050401(R) (2001); Y. Han and D. G. Grier, Phys. Rev. Lett. **91**, 038302 (2003).
[18] See supplementary material at http://link.aps.org/supplemental/10.1103/PhysRevLett.104.205703 for details.
[19] C. H. Mak, Phys. Rev. E **73**, 065104(R) (2006).
[20] J. C. Crocker and D. G. Grier, J. Colloid Interface Sci. **179**, 298 (1996).
[21] P. N. Pusey, Science **309**, 1198 (2005).
[22] C. A. Murray and D. H. Van Winkle, Phys. Rev. Lett. **58**, 1200 (1987); A. H. Marcus and S. A. Rice, *ibid.* **77**, 2577 (1996).
[23] P. N. Pusey and W. van Megen, Nature (London) **320**, 340 (1986).
[24] R. Messina and H. Löwen, Phys. Rev. Lett. **91**, 146101 (2003); R. Messina, J. Phys. Condens. Matter **21**, 113102 (2009).
[25] P. J. Steinhardt, D. R. Nelson, and M. Ronchetti, Phys. Rev. B **28**, 784 (1983).
[26] S. Neser *et al.*, Phys. Rev. Lett. **79**, 2348 (1997).